Characterizing Pathologically Relevant Mutations in Human Plastin 3 (PLS3)

Undergraduate Research Thesis

Presented in fulfillment of the requirements for graduation *with research distinction* from The Ohio State University's College of Pharmacy BSPS program

By

Matthew Orchard

The Ohio State University

April 2020

Project Advisor:
Dr. Dmitri Kudryashov
Department of Chemistry and Biochemistry

Contributing members:
Dr. Christopher Schwebach
Dr. Elena Kudryashova
Lucas Runyan

Table of Contents

*includes any methods M.O. performed, or was trained in

Vita

2012-2016……St. John's Jesuit High School & Academy, Toledo, OH

2016-2020……The Ohio State University, Columbus, OH

Fields of Study

Major: Pharmaceutical Sciences

Area of Distinction: Biochemistry

Acknowledgements

I am grateful for all of the members of the Kudryashov group for their endless patience and support throughout my time conducting biochemistry research here. Over the past three years of my undergraduate research experience, I have been blessed to be mentored by Dr. Dmitri Kudryashov, Dr. Elena Kudryashova, Dr. Christopher Schwebach, and the other graduate students. Being a part of the scientific process has given me valuable insight, and immense critical analyzing and reasoning skills that not only developed my well-rounded education here at The Ohio State University, but also will aid me towards future directions in the field. Firstly, I would like to thank my mentor, Dr. Dmitri Kudryashov, who took me under his wing as a sophomore with little research experience and guided me throughout the entirety of my time conducting research. Secondly, I would also like to thank Dr. Elena Kudryashova, Dr. Christopher Schwebach, and Lucas Runyan. My additional mentors provided guidance, advice, criticism, technical assistance and much more that aided me in becoming a better researcher and a better person. Without all of my incredible mentors, writing this thesis would not have been possible. Lastly, I would like to thank the other graduate and undergraduate students of the Kudryashov group, who provided friendly memories, technical assistance or advice at one point or another. Overall, every person part of the Kudryashov group made my time at The Ohio State University a memorable one, and for that I am eternally indebted.

Chapter 1 – Introduction

1.1 The Actin Cytoskeleton

Actin is the most abundant intracellular protein in eukaryotes, comprising up to 10 percent of the total protein by weight in muscle cells, and up to 5 percent in non-muscle cells (Lodish et. al., 2000). Actin is a highly conserved cytoskeletal protein and plays a major role in cytokinesis, motility, contractility, vesicle trafficking, cellular polarization, and forming cellular junctions (Perrin & Ervasti, 2010). Actin's involvement in various functions allows for cells to maintain homeostasis and function through interacting with their environment.

Monomeric actin (G-actin) is a globular protein stabilized by binding adenosine triphosphate (ATP) or diphosphate (ADP) in its cleft. G-actin can polymerize to form polar, helical, and dynamic filaments (F-actin, microfilaments). The rate-limiting step in the polymerization process is a formation of a stable nucleus of three actin subunits (Pollard & Craig, 1982). Once the stable nucleus is formed, polymerization will occur at two distinct filament ends, the pointed (-) end and the barbed (+) end. Both polymerization and depolymerization rates are faster at the more dynamic barbed end, although polymerization is prevailed at the barbed end (Lodish et. al., 2000). Actin polymerization is a reversible process driven by the hydrolysis of ATP catalyzed by actin's ATPase activity, and thus all F-actin subunits contain either bound ADP, ADP + P_i, or ATP (Straub & Feuer, 1950; Kudryashov & Reisler, 2013). F-actin polarity is determined by the association of ATP-actin to one end (freshly polymerized actin, preferentially at the barbed end) and dissociation of ADP-actin from the other end ("aged" actin, preferentially from the pointed end). When the net rate of the addition of G-actin to the barbed end equals the rate of the dissociation of G-actin from the pointed end, this is recognized as steady-state conditions and the filament is said to be "treadmilling" (Pratt & Cornely, 2014; Figure 1). Treadmilling allows for

the recycling of ADP-bound G-actin for ATP-bound G-actin and is a key factor in sustaining a multitude of cellular activities including cell motility, cell adhesion, and cell shape maintenance.

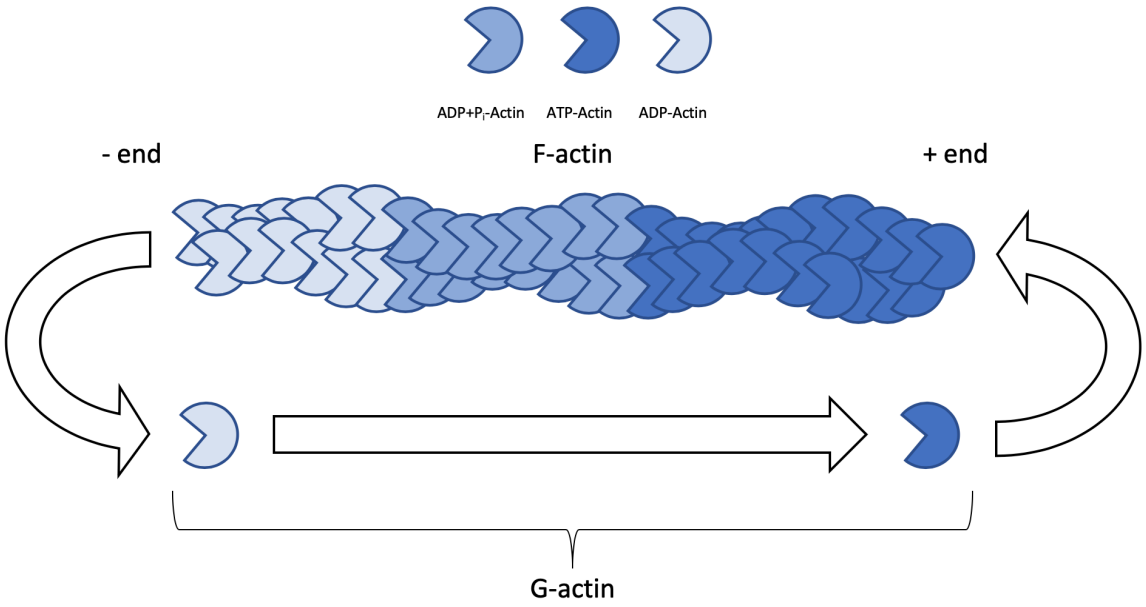

Figure 1: Actin Treadmilling
ATP-actin is added at the + end (barbed end) of the F-actin filament. Actin's ATPase activity results in the formation of ADP+P_i-actin subunits. Once P_i is released from the actin subunits, ADP-actin is formed before dissociation from the filament's – end (pointed end).

However, spontaneous actin polymerization does not occur in the cell. All steps of actin dynamics are strictly controlled spatially and temporally by numerous actin-binding proteins (ABPs) to allow the formation of various actin structures adapted to specific cellular functions. ABPs regulate polymerization, depolymerization, nucleation, branching, and cross-linking of F-actin (Pollard & Cooper, 2009). Actin cross-linking proteins aid in maintaining the shape of the actin cytoskeleton by incorporating F-actin into highly ordered networks (Figure 2). How F-actin is organized into these networks determines the classification of these proteins, including actin-bundling and web-forming proteins. Web-forming proteins, such as filamin, organize actin into intertwined, orthogonal mesh networks (Figure 2b). These networks are found in the cortical

cytoskeletal region adjacent to the plasma membrane and mainly support the cell surface (Cooper, 2000).

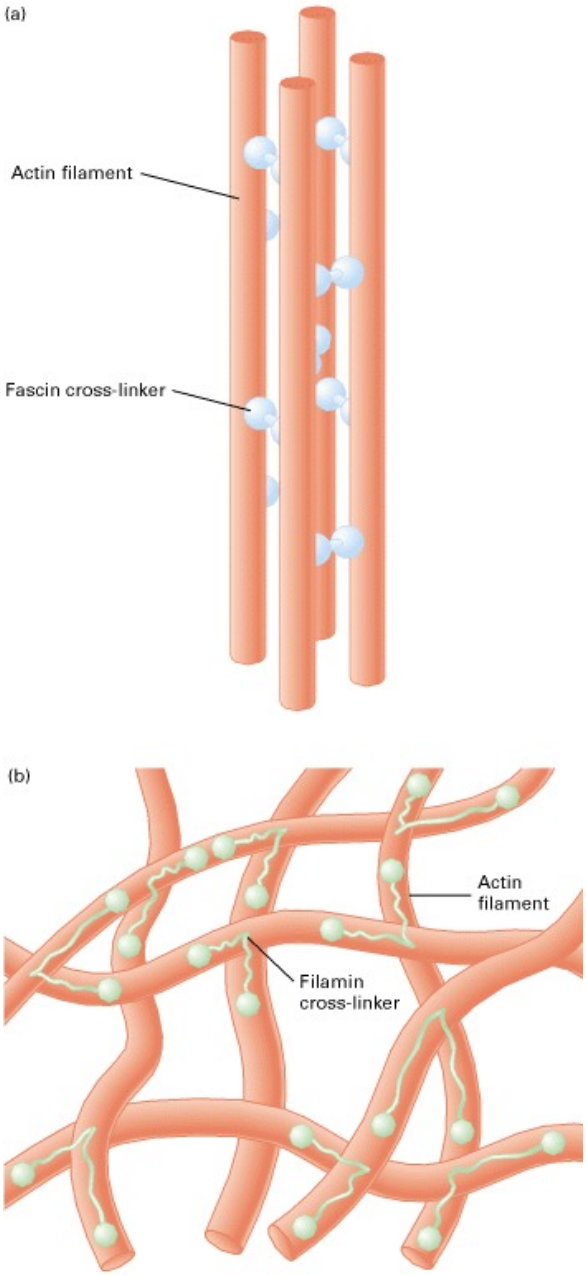

Figure 2: Actin Web vs. Bundled Networks (Lodish et. al., 2000)
(a) Actin bundles are formed by crosslinkers that organize the filaments into tight, parallel networks with the same (parallel) or opposite (antiparallel) polarities.
(b) Actin web networks are formed by crosslinkers that organize the filaments into intertwined, orthogonal mesh networks.

Actin-bundling proteins (Figure 2a), such as fascin and plastin, organize actin into tight, parallel networks with the same polarity (e.g., as in microvilli of intestinal brush border epithelial cells (Lin et. al., 1994)), although plastin (more commonly referred to as fimbrin in yeast) supports the formation of anti-parallel bundles as well (Skau et. al., 2011). Actin bundles are found in various cellular projections, including microvilli, focal adhesions, and at the leading edge of motile cells in filipodia (Bartles, 2000; Cooper, 2000). Additionally, they are found to form stress fibers, which are contractile acto-myosin structures comprising of antiparallel actin filament bundles, which provide cell anchorage and contractile movement (Cooper, 2000; Mitchison & Cramer, 1996). The topic of this thesis focuses on the association and functionality of the actin-bundling protein, plastin, which is involved in relevant human diseases.

1.2 Plastin Function and Regulation Within Cells

Plastins are an evolutionarily conserved family of actin-bundling proteins that are responsible for forming cross-linked actin networks used for motile cellular projections, such as lamellipodia in macrophages and invadopodia in metastatic tumors, and attachment, such as focal adhesions in osteoblasts (Arpin et. al., 1994; Adams et. al., 1995; Lommel et. al., 2016; Kamioka et. al., 2004). Plastins' domain structure (Figure 3) comprises a regulatory domain with two calcium-binding EF-hands and a core containing two actin-binding domains (ABD1 and ABD2), each of which can bind to a separate actin filament. Such architecture is unique among other ABPs: two consecutive ABD's within a single polypeptide chain enables the ability of plastins to bundle F-actin without the need for homodimerization (Shinomiya, 2012). This is in contrast to other actin-bundling proteins, such as α-actinin, containing only one ABD, and, therefore, requiring antiparallel homodimerization for bundling of F-actin (Addario et. al., 2016). The ABDs can be further broken down into calponin-homology domains 1-4 (CH1, CH2, CH3 and CH4, Figure 3),

which consist of about 125 residues each, first identified in calponin, an actin-binding protein involved in muscle contraction (Lodish et. al., 2000; Shinomiya, 2012).

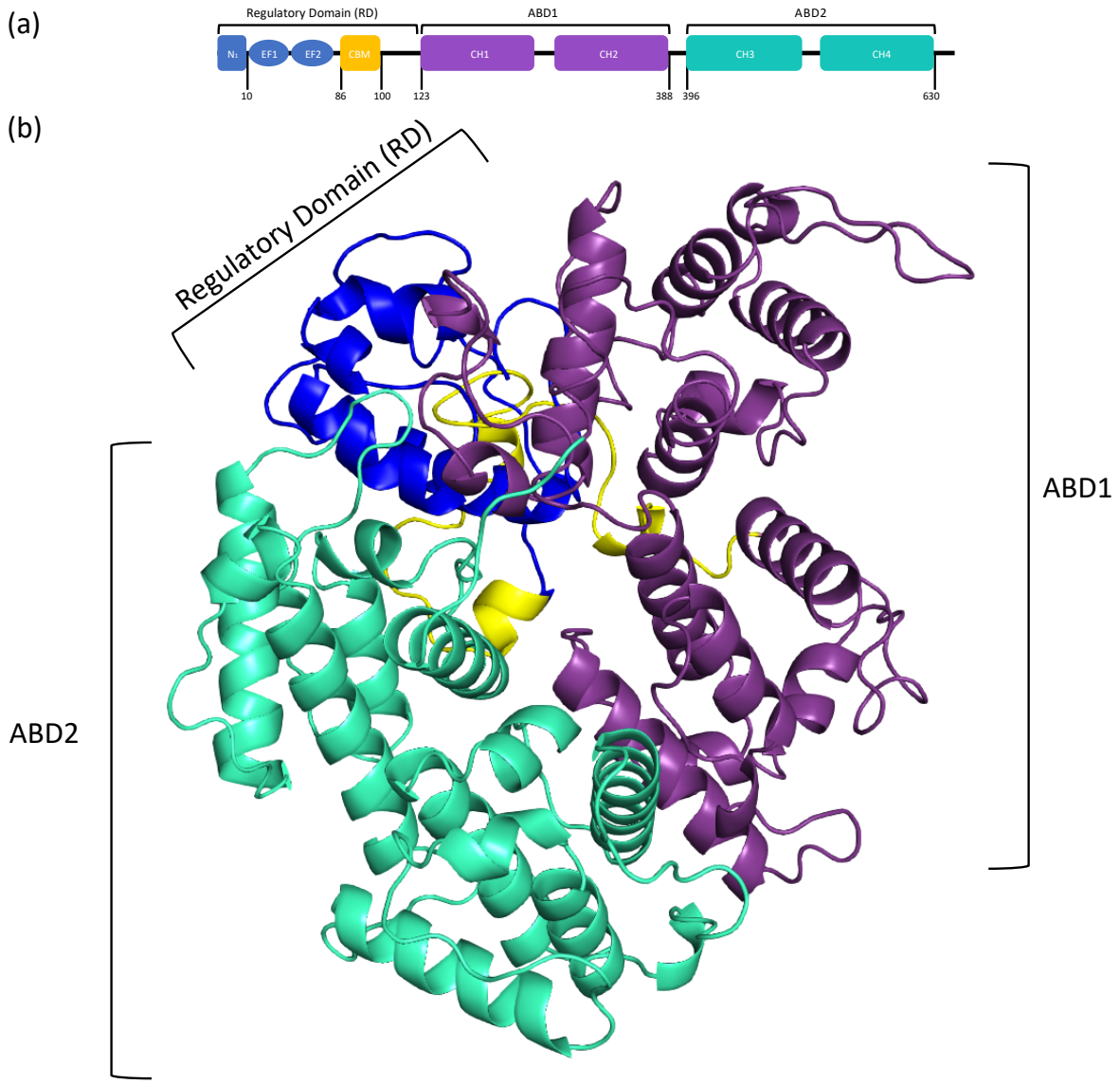

Figure 3: Domain structure of PLS3
A linear scheme of PLS3's domains (a) and a homology-modeling structure of PLS3 (Phyre) (b) are shown (domain coloring scheme is the same in both representations). The regulatory domain (RD) contains the N-terminal region (N), two Ca^{2+}-binding EF hands, and a calmodulin-binding motif (CBM). Each pair of four tandem calponin-homology domains (CH1-4) composes two actin-binding domains (ABD1 and ABD2).

Vertebrates express three different plastin isoforms in a tissue-specific manner with a 74-80% amino acid sequence similarity: PLS1 (or I-plastin), PLS2 (LCP1 or L-plastin) and PLS3 (or

T-plastin) (Shinomiya, 2012). PLS1 is primarily expressed in the microvilli of the intestinal brush border epithelium, in the stereocilia of the auditory hair cells of the inner ear, and in the kidney epithelium (Lin et. al., 1994; Drenckhahn et. al., 1991). Mutations in PLS1 cause autosomal dominant nonsyndromic hearing loss (Diaz-Horta et. al., 2019; Schrauwen et. al., 2019). PLS2 is primarily found in cells of hematopoietic origin (lymphocytes, macrophages, granulocytes) and is critical for proper innate and adaptive immune cell functioning (Shinomiya, 2012; Shinomiya et. al., 1995; Hagi et. al., 2006). Intriguingly, PLS2 expression is induced in many cancer cell types of non-hematopoietic origin (Lin et. al., 1993), where it is believed to aid tumor cells in migration and metastasis, and this impact is dependent on the phosphorylation status of PLS2 (Ripligner et. al., 2014). PLS3 is ubiquitously expressed in most solid tissues, while its aberrant expression is found in some cancers (Lin et. al., 1993). Mutations in PLS3 cause hereditary osteoporosis (Kämpe et. al., 2017; van Dijk et. al., 2013; Fahiminiya et. al., 2014; Nishi et. al., 2016) and congenital diaphragmatic hernia (CDH; Longoni et. al., 2019), which are the main topic of the present thesis (described in detail in Chapter 1.3). Additionally, PLS3 is believed to be crucial in development, as it was found to be the primary plastin isoform expressed in zebrafish embryos and has been reported as a protective modifier of spinal muscular atrophy, which is a developmental disease (Oprea et. al., 2008).

Plastin activity is subjected to regulation by several different mechanisms. One of the regulation modes is calcium binding to the EF-hands in the regulatory domain. Previous lab data has illustrated that increasing calcium concentrations inhibit the plastin-mediated formation of actin bundles by preventing ABD2 from binding to an actin filament, but has no impact on ABD1 binding (Schwebach et. al., 2017). The second mode of regulation involves phosphorylation, which has been most studied in PLS2 (Shinomiya et. al., 1995). Specifically, phosphorylation of Ser5 *in*

cellulo occurs upon stimulating macrophages with LPS, and has been shown to increase F-actin bundling by PLS2 (Janji et. al., 2006; Shinomiya et. al., 1995). However, phosphorylation-mimicking mutations (S5D or S5E) had no significant effect on PLS2's actin bundling ability *in vitro* (Schwebach et al., 2017) suggesting an involvement of cellular partner(s) to mediate the PLS2 phosphorylation-induced effects *in cellulo*. Ser5 phosphorylation has also been found in cells upon stimulation of T lymphocyte receptors (Henning et. al., 1994). Ser7 phosphorylation has also been reported *in vitro* and in cells (Morley, 2012). Interestingly, many other phosphorylation sites (primarily S and Y residues) in all three isoforms have been reported based on *in vivo* proteomic assays (PhosphoSitePlus; Hornbeck et. al., 2012). However, most identified phosphorylation sites have not been extensively investigated. Phosphorylation of PLS2 is believed to activate its ability to localize at actin-rich structures and to bundle actin, as suggested by the localization of phosphorylated PLS2 to migratory structures in cells (Lommel et. al., 2016). Therefore, different modes of plastin regulation enable fine-tuning of plastin localization and functioning for proper cellular activity, and its dysregulation can result in disease pathologies.

1.3 Plastin 3 Involvement in Congenital Diseases

Plastins have been linked to numerous diseases, including cancer (Riplinger et. al., 2014; Lommel et. al., 2016), spinal muscular atrophy (Yanyan et. al., 2014), hearing impairment (Diaz-Horta et. al., 2019), and neurodegenerative diseases (Ralser et. al., 2005). Mutations in *Pls3*, which is the gene that encodes for PLS3, were found in patients with X-linked osteogenesis imperfecta (OI or congenital osteoporosis; Kämpe et. al., 2017; van Dijk et. al., 2013; Fahiminiya et. al., 2014; Nishi et. al., 2016) and congenital diaphragmatic hernia (CDH; Longoni et. al., 2019), which are the primary topic of this thesis (Figure 4).

X-linked osteogenesis imperfecta (OI) is characterized by disrupted bone microarchitecture and low bone mineral density resulting in numerous fractures with variable severity, and increased bone fragility (van Dijk et. al., 2011). Most cases of OI result from genetic mutations in collagen type Iα1 (*COLIA1*) and Iα2 (*COLIA2*; van Dijk et. al., 2013). Other cases of OI are linked to post-translational modifications, intracellular transport, extracellular matrix incorporation, or altered protein folding of collagen (Forlino et. al., 2011). However, over 20 different novel mutations in *Pls3* have been found in patients with OI, and the role of PLS3 in OI has not been previously characterized. Of the >20 reported *Pls3* mutations, only 5 result in full-length PLS3 protein expression (Figure 4).

(a)

PLS3 OI mutations	PLS3 CDH mutations
E249_A250insI-L	E270K
A253_L254insN	W499C
A368D	M592V
N446S	
L478P	

(b)

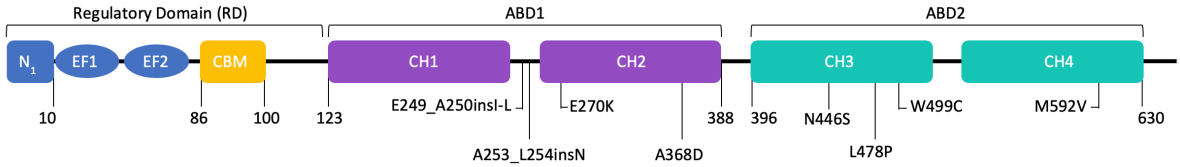

Figure 4: PLS3 Disease-Associated Mutations resulting in full-length protein expression
Above are listed the mutations in PLS3 (a) and their position in PLS3 domain structure (b). Each are found in patients with either osteogenesis imperfecta (OI) or congenital diaphragmatic hernia (CDH). PLS3 E249_A250insI-L mutation is a 12-amino acid insertion as followed: IMGHSHSGSCLL.

Congenital diaphragmatic hernia (CDH) is a human development impairment that is characterized by improper formation of the diaphragm, which separates the thoracic cavity from the abdominopelvic cavity. In CDH patients, the diaphragm defects cause the contents of the abdomen moving up into the thoracic cavity during breathing (Donahoe et. al., 2016). CDH is associated with a high mortality and morbidity in infants usually secondary to severe respiratory

failure linked to pulmonary hypoplasia and persistent pulmonary hypertension. Although the link between CDH and respiratory failure is known, its pathogenesis is not quite well understood (Keijzer & Puri, 2010). Many gene candidates have been linked to disturbing diaphragm and lung development in animal models, and CDH is believed to be polygenic (Donahoe et. al., 2016). Often, disruption of pleuroperitoneal folds development results in incomplete diaphragm morphogenesis and consequently herniation (Ameis et. al., 2017). Three novel mutations in *Pls3* resulting in full-length protein expression were found in patients (Longoni et. al., 2019; Figure 4), and the role of PLS3 in CDH is not clearly understood as well.

PLS3's involvement in OI and CDH is intriguing, since the mutations occur in the same protein in different tissues, although of the same mesenchymal origin. Thus, it is unclear why mutations in the same protein would not result in symptoms of OI and CDH simultaneously. Regardless, the manifestation of these diseases could be a result of the intricate changes in the tertiary structure of PLS3 for which proper regulation and function is altered. Additionally, it is possible that the expression of the mutated PLS3 is induced after differentiation of the mesenchymal cells into tissues. The particular mutated PLS3 residues must be crucial overall for proper functioning, since the mutations result in altered, maladaptive phenotypes in patients. Knockout mice and knockdown zebrafish studies have highlighted the importance of PLS3 in the development of bone and connective tissue (van Dijk et. al., 2011; Yorgan et. al., 2020; Dor-on et. al., 2017). However, the role(s) of *Pls3* mutations in the congenital diseases of OI and CDH has not been elucidated. Overall, plastins' involvement in human disease states illustrates the importance of researching the family of proteins in order to develop a deeper understanding for biomedical advancement, and thus proposes plastins as a possible therapeutic target.

Chapter 2 – Results

2.1 Effects of the Disease-Related Mutations on the PLS3 Protein Stability

In order to first elucidate the link between PLS3 and OI and CDH pathologies, effects of the respective mutations on PLS3 stability was assessed by differential scanning fluorimetry (DSF). DSF can be utilized to obtain a melting temperature of each protein, which can be utilized as a measure for protein stability (Niesen et. al., 2007). To this end, wild-type (WT) and mutated PLS3 proteins were expressed and purified from *Escherichia coli* as recombinant 6xHis-tagged constructs. None of the CDH-related PLS3 mutants exhibited a statistically significant difference in melting temperature with respect to WT PLS3 (Figure 5a,b), although, W499C was the most destabilizing mutation (by 3.44°C, compared to WT). The OI-related mutants exhibited various degrees of destabilization compared to WT, which was evident from the decrease in the melting temperatures of the mutated PLS3 ranging from 2.6-7.6°C (Figure 5c,d). However, the melting temperatures for all studied proteins were found to be well above physiological temperature (37°C), suggesting that all the mutated PLS3 proteins are able to maintain their tertiary structure at physiological conditions. This implies that the OI and CDH pathologies caused by the tested mutations do not stem from the reduced PLS3 protein stability.

(a)

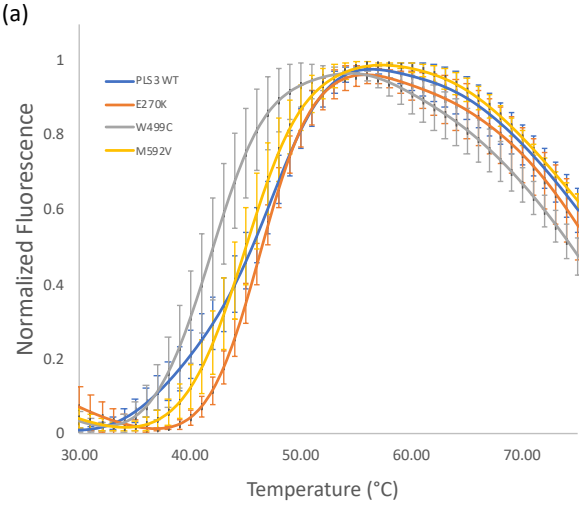

(b)

CDH PLS3 Mutants		
Melting Temperature (°C)		***p*-values**
PLS3 WT	46.25 ± 1.24	
E270K	46.91 ± 0.92	0.0904
W499C	42.81 ± 2.69	0.1472
M592V	45.28 ± 1.82	0.1861

(c)

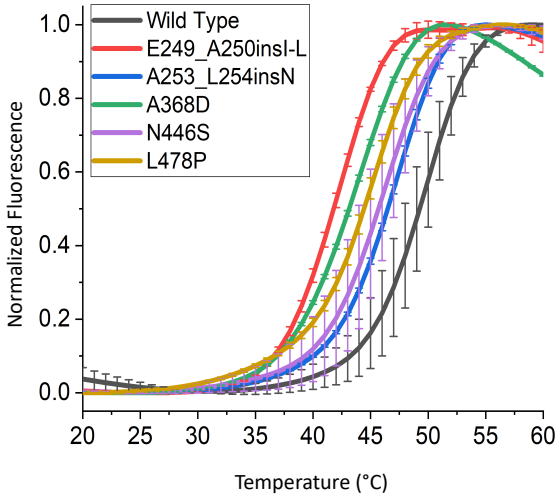

(d)

OI PLS3 Mutants		
Melting Temperature (°C)		***p*-values**
PLS3 WT	49.47 ± 1.25	
E249_A250insI-L	41.93 ± 0.32	0.0005*
A253_L254insN	46.87 ± 0.12	0.0228*
A368D	43.38 ± 0.08	0.0011*
N446S	45.94 ± 1.64	0.0413*
L478P	44.93 ± 0.27	0.0035*

Figure 5: Stability of PLS3 CDH and OI mutants
Shown above are the melting profiles of the PLS3 CDH (a, b) and OI (c, d) mutants. DSF melting profiles were utilized as a readout for stability by assessing protein unfolding in the presence of a fluorescent probe (Sypro Orange), fluorescence of which is enhanced by binding to the protein's exposed hydrophobic residues upon thermal denaturation. None of the PLS3 CDH mutants were significantly destabilized compared to WT PLS3. The PLS3 OI mutants expressed various degree of minor destabilization compared to WT PLS3 (ranging from 2.6-7.6°C). *p*-value was calculated by comparing each mutated PLS3 data set (n=3) with the WT data set (n=3) using Student's *t*-test (two-tailed distribution, equal variance). Asterisks indicate a statistically significant difference ($p<0.05$).

2.2 Effects of the Disease-Causing PLS3 Mutations on Actin Binding and Bundling Abilities of PLS3

The actin binding and bundling capabilities of WT and mutated PLS3 proteins were tested by utilizing high-speed and low-speed co-sedimentation assays, respectively (Schwebach et. al., 2017). Centrifugation at high-speed (300,000 g) allows for the separation of F-actin pelleted together with bound PLS3, while leaving unbound PLS3 in the supernatant. Centrifugation at low-speed (17,000 g) allows for the separation of F-actin bundles in the pellet and single actin filaments in the supernatant.

Our lab's studies have previously revealed that ABD1 is the primary F-actin binding domain regardless of Ca^{2+} concentration, while PLS3-mediated F-actin bundling occurs only at low Ca^{2+} concentration, when ABD2 is not inhibited by RD and also available for F-actin binding together with ABD1 (Schwebach et al., 2017). Thus, the actin binding abilities of all the PLS3

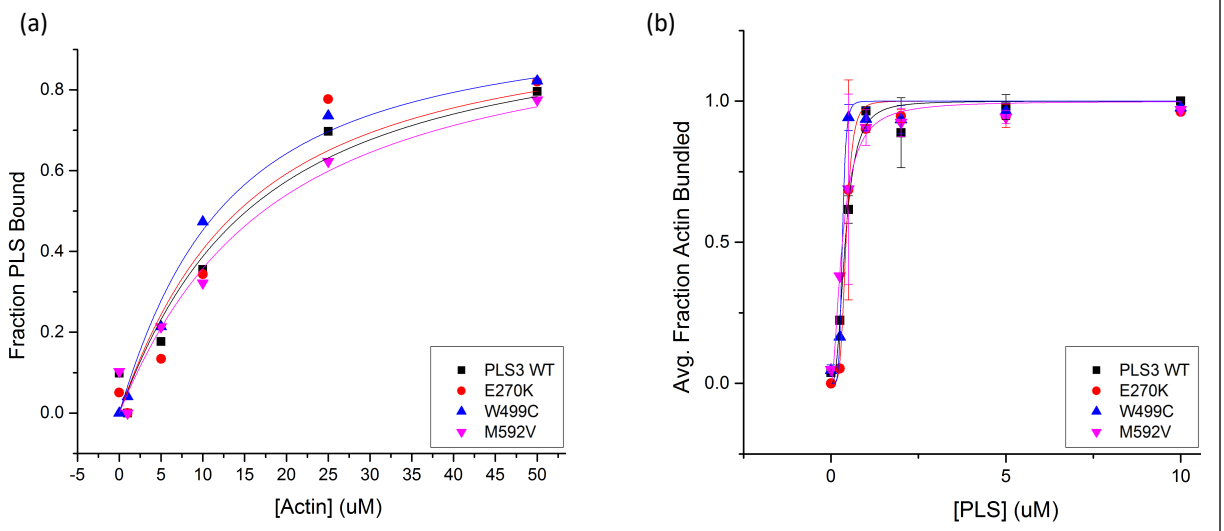

Figure 6: Binding and bundling abilities of PLS3 CDH mutants
The ability of each mutant to bind or bundle F-actin was assessed by high- or low-speed co-sedimentation assays, respectively. All of the PLS3 CDH mutants and PLS3 WT bound to F-actin with similar affinities (a). The bundling ability of the mutants and WT PLS3 were similar as well under EGTA conditions (b). Further experiments are needed to validate these results.

constructs were first examined. All the OI- and CDH-related PLS3 mutants were able to bind to F-actin with affinities similar to the WT PLS3 value (Figures 6a & 7). The binding of the CDH-related mutants to F-actin was only examined once, and, therefore, it should be replicated in order to validate these results.

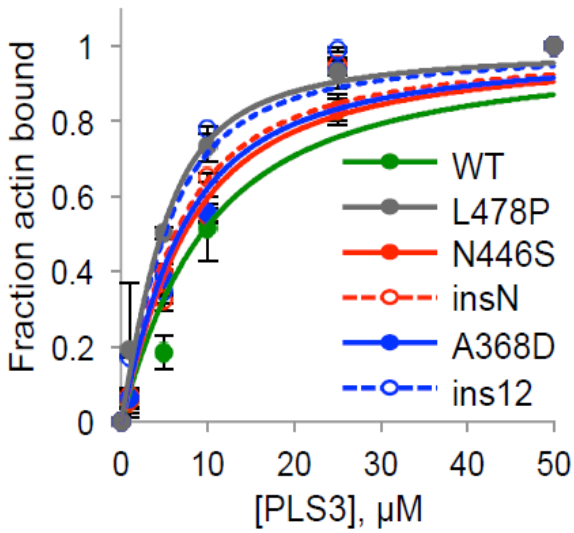

(b)

	K_d (µM)
PLS3 WT	7.95 ± 2.51
E249_A250insI-L	2.55 ± 0.86
A253_L254insN	3.76 ± 0.96
A368D	4.21 ± 0.95
N446S	4.76 ± 0.77
L478P	2.15 ± 0.31

Figure 7: Binding abilities of PLS3 OI mutants
The ability of each mutant to bind F-actin was assessed by high-speed co-sedimentation assays. All mutants retain their ability to bind F-actin. Of note, all mutants bound F-actin with a higher affinity compared to WT.

Next, the bundling capabilities of PLS3 constructs were assessed in the absence (chelated by EGTA) or presence of Ca^{2+}, which inhibits F-actin bundling by PLS3. It was found that the CDH-related mutants all bundle F-actin similarly to WT PLS3 under EGTA conditions. These experiments should be repeated in order to validate these results. The OI-related mutants exhibited similar bundling abilities compared to PLS3 WT under EGTA conditions, with the exception of L478P and E249_A250ins12I-L (Figure 8). The splice variant protein E249_A250insI-L exhibited a 4-fold increase in bundling ability compared to WT PLS3, while L478P could not bundle F-actin. Moreover, the OI-related mutants exhibited various bundling abilities in the presence of Ca^{2+}

compared to WT PLS3 (Figure 8). A368D and E249_A250insI-L both bundled F-actin more

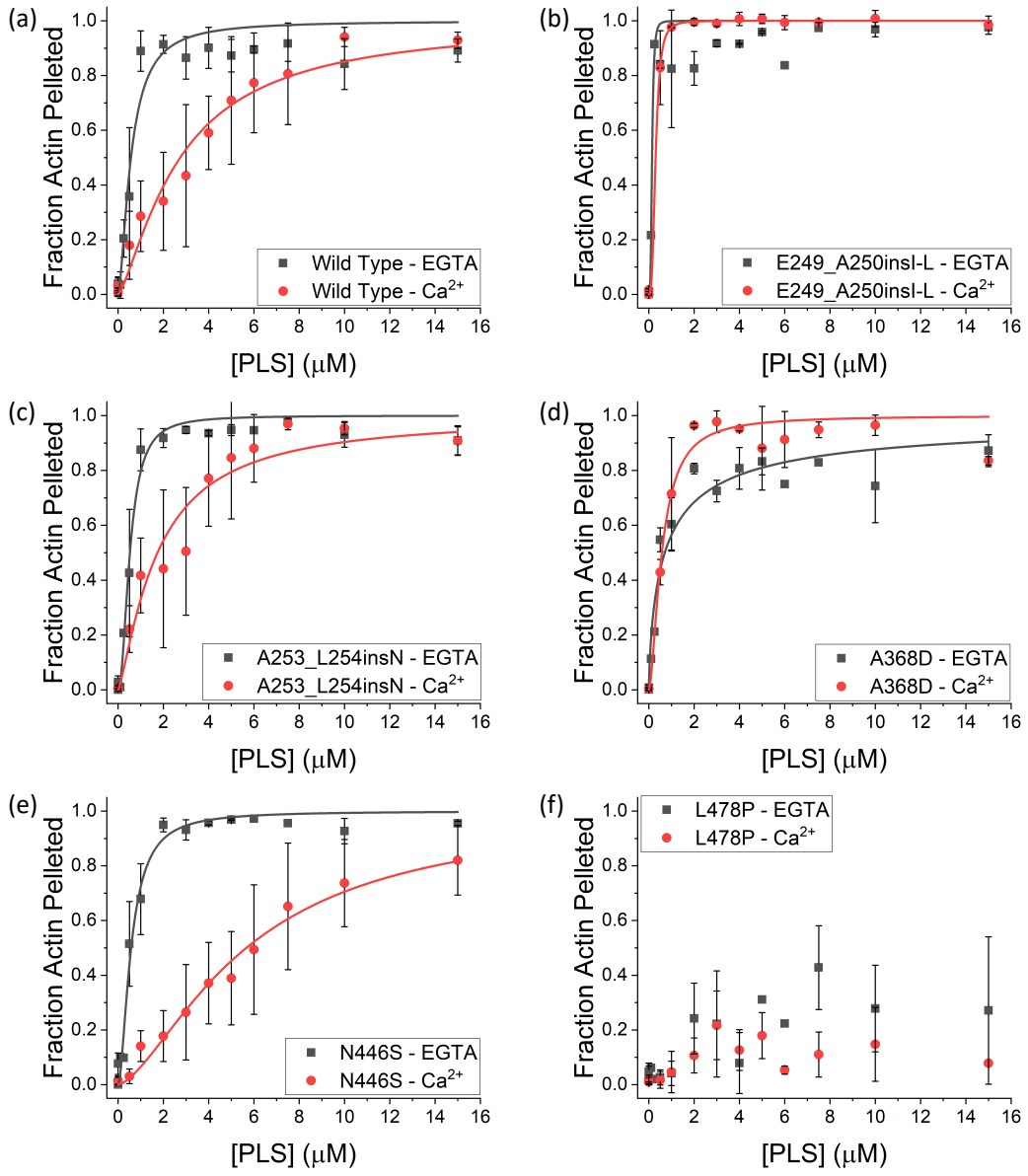

(g)

[PLS] (μM) at 50% Bundled Actin	EGTA	Ca^{2+}
PLS3 WT	0.57 ± 0.09	2.74 ± 0.23
E249_A250insI-L	0.14 ± 0.02	0.30 ± 0.03
A253_L254insN	0.52 ± 0.04	1.74 ± 0.23
A368D	0.70 ± 0.13	0.57 ± 0.08
N446S	0.58 ± 0.05	5.67 ± 0.23

Figure 8: Bundling of F-actin by PLS3 OI mutants
F-actin bundling by PLS3 OI mutants and PLS3 WT was tested by low-speed co-sedimentation assays. A368D and E249_A250insI-L bundle F-actin more effectively than WT under Ca^{2+} conditions. N446S bundles F-actin less effectively than WT under Ca^{2+} conditions. L478P could not bundle actin under both conditions tested. Under EGTA conditions. Under EGTA conditions, E249_A250insI-L and A253_L254insN bundled F-actin more effectively than WT.

effectively than WT PLS3. N446S bundled F-actin less effectively than WT PLS3, and A253_L254insN bundled F-actin similarly to WT PLS3 (Figure 8). These results suggest that Ca^{2+} sensitivity might be affected in the OI and CDH PLS3 mutants, which may result in altered protein ability to behave properly in individuals with OI or CDH.

2.3 Effects of the PLS3 Osteogenesis Imperfecta Mutations on Ca^{2+} Sensitivity of PLS3

In order to test whether Ca^{2+} regulation of PLS3 is perturbed by the OI mutations, light scattering assays coupled with Ca^{2+} titration were performed. PLS3-mediated F-actin bundles effectively scatter light; as more Ca^{2+} is added, F-actin bundles dissociate due to PLS3 inhibition by Ca^{2+}, and less light is scattered through the sample, which can be recorded using spectrofluorometer (Figure 9). Both N446S and A253_L254insN were more sensitive to Ca^{2+} regulation compared to WT PLS3. This was surprising for A253_L254insN since under saturated Ca^{2+} conditions it showed actin bundling activity similar to the WT PLS3 bundling. Both A368D and E249_A250insI-L were insensitive to Ca^{2+} titrations; the slight, steady decrease in the signal can be explained by simple mixing that is performed after each Ca^{2+} addition. L478P previously showed no bundling activity, thus its calcium sensitivity could not be determined.

(a)

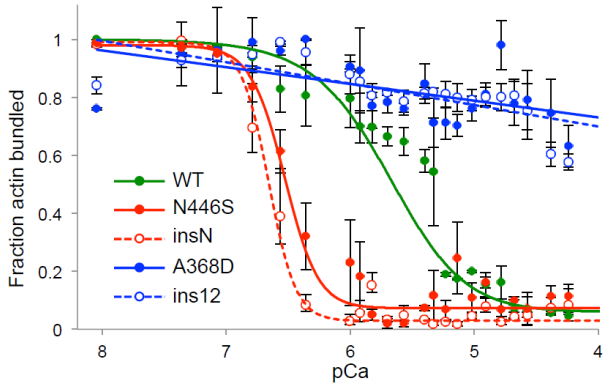

(b)

	pCa_{50}
PLS3 WT	5.46 ± 0.14
L478P	N/A
N446S	6.44 ± 0.21
InsN	6.66 ± 0.17
A386D	N/A
Ins12	N/A

Figure 9: Ca^{2+} sensitivity of PLS3 OI mutants
The dissociation of F-actin bundles was tested by light scattering upon titrating Ca^{2+} (a), which allowed us to determine pCa_{50} values (i.e., the concentration of Ca^{2+} where 50% of the F-actin bundles are dissociated) (b).

Overall, these experiments revealed that that the OI-PLS3 mutants can be categorized into three different groups: Ca^{2+}-hypersensitive (N446S and A253_L254insN), Ca^{2+}-insensitive (A368D and E249_A250insI-L), and bundling-incompetent (L478P). Additionally, this further illustrates the importance PLS3 F-actin bundling ability and its finely tuned Ca^{2+} regulation of PLS3.

2.4 Effects of the PLS3 Osteogenesis Imperfecta Mutations on PLS3 Cellular Localization

To test whether altered F-actin bundling ability and/or its impaired Ca^{2+} regulation in PLS3 disease-related mutants may alter their intracellular localization, mEmerald-tagged OI PLS3 mutants and WT PLS3 were expressed in spreading XTC fibroblasts (Figure 10) and in osteoblasts (U2OS) and osteocytes (Ocy454; data not shown). In addition to mEmerald-PLS3, the cells were co-transfected with mCardinal-tagged paxillin (focal adhesion marker) and mCherry-tagged

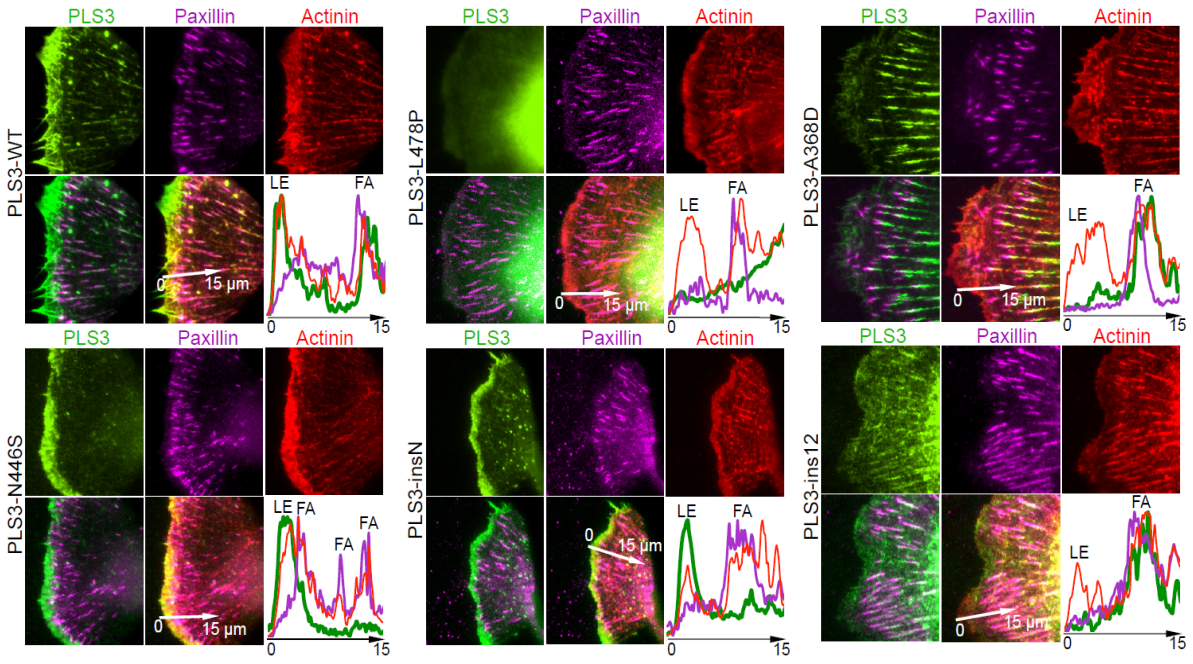

Figure 10: Differential subcellular localization of the PLS3 OI mutants
In spreading XTC fibroblast cells, WT PLS3 is equally distributed between the leading edge (LE) and focal adhesions (FA). The Ca^{2+}-insensitive mutants (A368D & E249_A250insI-L) preferentially localize to focal adhesions, while Ca^{2+}-hypersensitive mutants (N446S and A253_L254insN) preferentially localize the leading edge.

actinin (localizes to both, actin stress fibers and focal adhesions). WT PLS3 was found equally distributed between the focal adhesions and leading edge in all cell lines. Interestingly, PLS3 L478P was diffuse throughout the cytoplasm, and did not localize to any F-actin networks. This implies that PLS3-mediated F-actin bundling ability is necessary in order to associate with F-actin-rich cellular structures. The Ca^{2+}-insensitive and Ca^{2+}-hypersensitive mutants were found to preferentially localize to the leading edge and focal adhesions, respectively.

Ca^{2+} regulation is crucial for focal adhesion disassembly and recycling necessary for cell migration (Giannone et. al., 2004). Thus, it was investigated whether Ca^{2+} depletion (upon chelation of Ca^{2+} with EGTA) would further impact the localization of WT and mutated PLS3 (A368D and N446S; Figure 11). PLS3 A368D did not change its localization from the focal adhesions upon Ca^{2+} depletion. On the contrary, both PLS3 N446S and WT significantly redistributed from the leading edge to focal adhesions upon Ca^{2+} chelation. Overall, these results imply that OI-linked PLS3 mutations resulting in the impaired Ca^{2+}-regulation of PLS3 lead to altered cellular localization of the mutated PLS3 variants, thus affecting their proper functioning in OI patients.

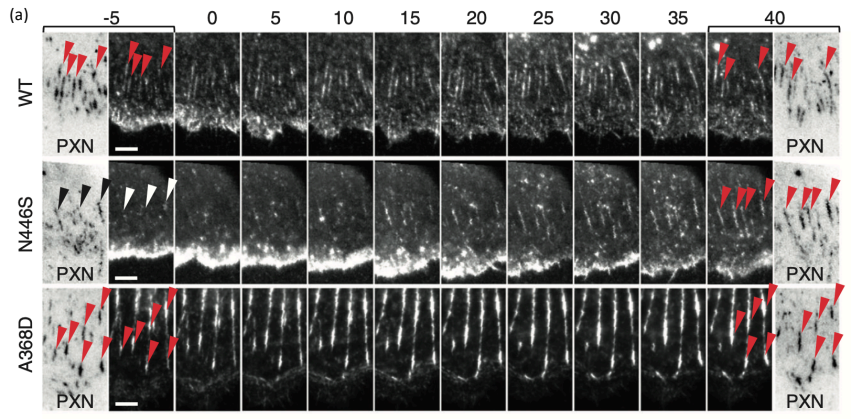

Figure 11: Redistribution of PLS3 WT and N446S upon Ca^{2+} depletion
In XTC fibroblasts, chelation of Ca^{2+} with EGTA (5 mM final concentration) caused a significant redistribution of PLS3 N446S and WT from the leading edge to focal adhesions. PLS3 A368D did not significantly redistribute upon Ca^{2+} chelation.

Chapter 3 – Discussion & Future Directions

The goal of this study was to characterize eight PLS3 mutations that result in the human diseases, osteogenesis imperfecta (OI) and congenital diaphragmatic hernia (CDH). Although the detailed molecular mechanisms underlying the PLS3-related disease pathologies is not known, our results revealed that PLS3 mutations affect the following aspects of PLS3 activity: (1) PLS3's ability to bundle F-actin, (2) the intricate Ca^{2+}-regulation of PLS3, and (3) the intracellular localization of PLS3.

Of the eight PLS3 mutants studied, only one (namely, L478P) lacked the ability to bundle F-actin into crosslinked networks. Thus, L478P is most similar to the PLS3 truncated, non-functional mutants reported in patients with OI (Fahiminiya et. al., 2014). Interestingly, F-actin binding affinity of PLS3 L478P was unperturbed by the mutation. Since PLS3 primarily binds to F-actin through ABD1, it is implied that PLS3 L478P binds to F-actin in the same fashion. Additionally, a cryo-EM structure of F-actin decorated with PLS2, which shares >80% identity with PLS3, suggests that PLS3 L478P is in close proximity to a tentative actin-PLS binding interface (Schwebach et. al., 2020). This further supports that PLS3 L478P binds to F-actin primarily through ABD1, and hindering its ability to bind through ABD2 is evident from the lack of F-actin bundling. Although PLS3 L478P could bind to F-actin, it lacked any association with F-actin-rich structures (e.g., focal adhesions, leading edge, stress fibers) in all tested cell lines (osteoblasts, osteocytes, and fibroblasts). This finding suggests that PLS3 must have the ability to bind to F-actin through both ABDs to fulfill its primary physiological function (e.g., bundle F-actin).

The three CDH PLS3 mutants (E270K, W499C, M592V) were able to bundle F-actin similarly to WT PLS3 under EGTA conditions. The bundling abilities of the CDH-related PLS3

mutants under Ca^{2+} conditions have not been thoroughly investigated. Upon an initial experiment, PLS3 E270K bundled F-actin more effectively than WT PLS3 under Ca^{2+} conditions (data not shown). Previously, it was predicted that these mutations may be classified as gain-of-function (Longoni et. al., 2019) Although these experiments were only performed once and should be validated through repetitions, these results suggest that these mutations may impact the Ca^{2+} regulation of PLS3, as observed with the OI-related mutants, and illustrate the importance of regulating PLS3's activity. Increasing or decreasing PLS3's ability to bundle F-actin through regulation could be detrimental to human body development, as observed in the CDH patients with the reported mutations (Longoni et. al., 2019). Alongside experimental repetitions exploring the CDH PLS3 mutants' sensitivity to Ca^{2+}, localization in cells should be explored. This would allow for further explanation of how perturbing PLS3's normal regulation in cells can reflect on dysfunction in cells and possibly CDH; specifically, whether the motility of cells is altered. Given PLS3's role in cellular motility, it was hypothesized that the motility of muscle progenitor cells, which is crucial for the morphogenesis of the diaphragm, could be altered by these mutations (Longoni et. al., 2019; Merrell & Kardon, 2013). Overall, initial findings illustrate that altered PLS3-mediated F-actin bundling ability (either decrease or increase with respect to WT PLS3) can result in dysfunction.

Perturbing PLS3's normal regulation is clearly apparent in the Ca^{2+}-hypersensitive (PLS3 N446S and A253_L254insN) and Ca^{2+}-insensitive (PLS3 A368D and E249_A250insI-L) mutants found in OI patients. Experiments assessing PLS3 OI mutants' bundling activity under Ca^{2+} conditions (performed by Lucas Runyan) and Ca^{2+} sensitivity (performed by Dr. Chris Schwebach) elucidated these categorical findings. Cellular experiments (performed by Dr. Elena Kudryashova) further emphasized these findings. PLS3's localization to actin structures was impaired by

perturbed Ca^{2+} regulation of PLS3-mediated F-actin bundling, and thus its proper functioning was limited. Intriguingly, while WT PLS3 was equally distributed between the leading edge and focal adhesions of cells, it was interesting to see that the Ca^{2+}-hypersensitive and Ca^{2+}-insensitive mutants primarily localized to the leading edge and focal adhesions, respectively. Additionally, the finding that Ca^{2+} promotes PLS3 redistribution from focal adhesions to the leading edge in cells illustrates the importance of balanced Ca^{2+} regulation of PLS3 and the intricate interplay between the PLS3 regulation and its intracellular localization.

Local rises in Ca^{2+} concentration allow for the disassembly and recycling of focal adhesions, which is necessary for migratory cells. Focal adhesion recycling is further accelerated by the recruitment of focal adhesion kinase (Giannone et. al., 2004). Since focal adhesions are essential for the migration of cells and formation of the extracellular matrix (e.g. bone; Diener et. al., 2005) and Ca^{2+} promotes PLS3 redistribution from focal adhesions to the leading edge, it is possible that PLS3 redistribution is a FAK-independent pathway aiding in focal adhesion recycling. Interestingly, chelating Ca^{2+} in cells resulted in PLS3 N446S redistributing from the leading edge to focal adhesions, while PLS3 A368D was retained at focal adhesions under Ca^{2+} or EGTA conditions. With rises in local Ca^{2+} concentration, osteoblasts expressing Ca^{2+}-insensitive PLS3 mutants would rely more on the FAK-dependent pathways for focal adhesion recycling, thus possibly hindering osteoblast migration and osteogenesis. Additionally, osteoblasts expressing Ca^{2+}-hypersensitive PLS3 mutants may have limited adhesion due to its preferred localization at the leading edge in the presence of Ca^{2+}, which could possibly impact the adhesion necessary for proper osteogenesis.

Besides its expression in osteoblasts, PLS3 is also expressed in osteocytes, which are the most abundant cells in bone. Osteocytes modulate bone turnover and remodeling by signaling and

regulating the activity of osteoclasts and osteoblasts. They are derived from active osteoblasts that are incorporated into the newly formed extracellular matrix and mature into the former (Tate et. al., 2004). Since PLS3 was prominent in osteoblasts and especially at bifurcations of the osteocyte dendritic processes, which are recognized as mechanotransducing structures (Kamioka et. al., 2004), it is possible that mutated PLS3 may impact the ability of osteocytes to sense and respond to mechanical stress. Thus, downstream signaling via non-canonical Wnt pathway, which is recognized as a central signaling pathway critical for osteoblastic differentiation (Galli et. al., 2010), could be negatively impacted resulting in the poor mineralization observed in OI.

Overall, all the results suggest that perturbed PLS3's regulation by Ca^{2+}, impaired localization to actin-rich structures, or compromised F-actin bundling ability possibly result in dysfunction(s) that manifests in the disease states OI and CDH, and proposes PLS3 as a potential therapeutic target.

Chapter 4 – Materials & Methods

4.1 F-actin Preparation

Monomeric rabbit or chicken skeletal muscle G-actin was prepared from acetone powder (Spudich et. al., 1971). G-actin was dialyzed in a buffer (5.0 mM Tris, pH 8.0, 0.2 mM $CaCl_2$, 0.2 mM ATP, 5.0 mM β-mercaptoethanol) and stored on ice for 4-6 weeks (dialyzing every 2 weeks). Prior to polymerization, Ca^{2+} bound to the nucleotide-binding cleft was chelated by adding 0.5 mM EGTA, and incubated on ice (10 min). This allowed for the exchange of Ca^{2+} for Mg^{2+} via the addition of 0.1 mM $MgCl_2$. Polymerization of Mg^{2+}-bound G-actin was induced by supplementation of $MgCl_2$ to 2 mM, KCl to 30 mM, and HEPES buffer (pH 7.0) to 10 mM, and allowed to proceed for 1 hour at 20-25°C before use.

4.2 DNA Cloning for Recombinant Protein Expression

PCR for amplification of PLS3 cDNA was run according to protocol (New England Biolabs) in a reaction mix containing 1X Q5 reaction buffer, 1X GC enhancer, 0.2 mM dNTPs, 0.5 μM of each forward and reverse primers, and 1 ng of PLS3-containing plasmid as a template. PCR was initiated by adding 0.25 units of Q5 High Fidelity Polymerase (New England Biolabs). The protocol included 30 seconds of initial thermal denaturation (98°C), 30 cycles of thermal denaturation (98°C, 10 seconds), annealing (55-72°C, 30 seconds), and extension (72°C, 30 seconds). The PCR product size was confirmed via agarose gel electrophoresis, and then purified using NucleoSpin Gel and PCR Clean-up kit (Takara Bio). The PCR product was then transformed into a modified pColdI expression vector, which allows for inducible, cold shock expression at

15°C, using NEBuilder HiFi DNA Assembly Master Mix (New England Biolabs). Successful PCR cloning was confirmed by Sanger Sequencing (Genomics Center of The James Comprehensive Cancer Center at OSU).

4.3 Site-Directed Mutagenesis

All PLS3 OI and CDH mutations were introduced into the plasmid pColdI-PLS3 by utilizing site-directed mutagenesis (SDM), except for E249_A250insI-L. Due to the size of this splice variant insertion, NEBuilder HiFi DNA Fragment Assembly Kit (New England Biolabs) was used to introduce the 12 amino acids (IMGHSHSGSCLL) into pColdI-PLS3 vector. Forward and reverse primers containing the desired mutations were designed and ordered (Sigma-Aldrich). The SDM protocol was performed in 1X Q5 reaction buffer, 1X GC enhancer, 0.4 mM dNTPs, 0.2 mM of each forward and reverse primer, and 25 ng template pColdI-PLS3. 0.5 units of Q5 High Fidelity Polymerase (New England Biolabs) was added in order to initiate each reaction. The protocol included an initial thermal denaturation (98°C, 2 min), 30 cycles of thermal denaturation (98°C, 1 min), annealing (55-72°C, 1 min), and extension (72°C, 8 min). After completion of the PCR cycle, the SDM product was digested with DpnI for 3 hours (37°C). DpnI digests the template DNA, which is methylated unlike the amplified PCR product, and thus only PCR-amplified DNA with an introduced mutation is leftover. This product is subsequently transformed into *E. coli* XL-10 Gold competent cells. Successful introduction of each mutation was verified by Sanger Sequencing (Genomics Center of The James Comprehensive Cancer Center at OSU). The same protocol was utilized to introduce all of the mutations into the pcDNA3-mEmerald PLS3 plasmid for mammalian expression in the cellular experiments.

4.4 Expression and Purification of Recombinant Wild-type and Mutated PLS3

Recombinant PLS3 WT and mutants were expressed via transforming each pColdI-PLS3 plasmid into BL21-CodonPlus *E. coli* competent cells. The cells were grown overnight (37°C) in nutrient-rich bacterial growth medium (MMI; 5 mL total volume, 2.5% yeast extract, 1.25% tryptone, 125 mM NaCl, 0.4% glycerol, 50 mM Tris-HCl at pH 8.2, 5 µL ampicillin, 5 µL chloramphenicol). The optical density of the culture was measured at 600 nm ($OD_{600\ nm}$). The cells were subsequently centrifuged (3,000 g's, 4°C, 10 min), the supernatants were decanted, and the pellets were resuspended in 1 mL MMI. The suspensions were inoculated in 500 mL of MMI (starting $OD_{600\ nm}$ of 0.1) with 500 µL of each aforementioned antibiotic. Cells were grown until an $OD_{600\ nm}$ of 1.0-1.2, chilled to 15°C on ice, and expression was induced by adding 1 mM IPTG and growing cells at 15°C, 250 rpm for 16 hours. The resulting cell cultures were centrifuged (3,000 g, 20 min, 4°C), and the pellets were resuspended in Buffer A (50 mM Hepes pH 7.4, 300 mM NaCl, 5 mM imidazole, 0.1 mM PMSF, 2 mM benzamidine, 1:500 trypsin inhibitor, 1:500 leupeptin/pepstatin inhibitor). Cell suspension was freeze/thawed in liquid nitrogen 3 times, and sonicated 3 times (80% amplitude, 10 s pulse with 10 s interval for 2 min). The cell lysate was centrifuged (Beckman Type 70 Ti rotor, 25,000 rpm, 4 °C, 25 min), and filtered through cellulose filter paper. Since each protein contained 6X-His tag located at the N'-terminus, the proteins were purified via metal affinity purification. The cleared cell lysate was nutated with TALON cobalt resin beads (Takara) for 3 hours at 4 °C before loading into a gravity column. Three washes (50 mL) were performed on the resin in the column with increasing concentrations of imidazole. Imidazole is used to elute resin-bound 6xHis-tagged proteins due to its structural similarity to the histidine side chain, which competes with 6xHis-tag for binding with the cobalt (or nickel) resin. The eluted fractions were

analyzed via SDS-PAGE. Target elution fractions were concentrated and dialyzed overnight (4°C) against storage buffer (10 mM HEPES pH 7.0, 30 mM KCl, 2 mM $MgCl_2$, 0.5 mM EGTA, 2 mM DTT, 0.1 mM PMSF). Protein samples were aliquoted (55 µL), frozen in liquid nitrogen, and stored (-80°C) until use.

4.5 High-Speed and Low-Speed Co-sedimentation Assays

Before use, 1 µL of 0.5 M TCEP was added to PLS3 aliquots to reduce cysteines, and placed on ice (30 min) before centrifugation (300,000 g, 30 min, 4°C) to remove protein aggregates. Protein concentrations in the supernatant were determined via UV-visible absorption spectroscopy at 280 nm using extinction coefficients determined by web-based ProtParam tool (ExPASy). F-actin was polymerized from monomeric G-actin as described above. High-speed binding reactions included either 5 µM plastin and varying concentrations of F-actin (0-50 µM) in PLS buffer (10 mM HEPES pH 7.0, 30 mM KCl, 2 mM $MgCl_2$, 0.5 mM EGTA, 2 mM DTT, 0.1 mM PMSF). Low-speed bundling reactions were performed in the presence of either 5 µM or 2 µM F-actin and varying concentrations of plastin (0-10 µM) in PLS buffer. When necessary, $CaCl_2$ was added to the reactions to yield a final free Ca^{2+} concentration of 0.5 mM as calculated (Schoenmakers et. al., 1992). Binding and bundling reactions were either incubated at 4°C overnight then for 1 hour at room temperature (20-25°C), or for 3 hours at room temperature before subsequent centrifugation. Binding and bundling reactions were centrifuged at high speed (300,000 g for 30 min) or low speed (17,000 g for 15 min), respectively (25°C). Supernatants were separated from the pellets, pellets were resuspended in 1X SDS-sample buffer, and supernatants were supplemented with 4X SDS-sample buffers making sure both fractions had equal final volumes. Samples were resolved on 9%

SDS-PAGE, and analyzed using ImageJ processing software (NIH). Bundling reactions were fit to the Hill equation:

$$\%\ Actin\ Bundled = \frac{[PLS]^n}{{K_A}^n + [PLS]^n}$$

$$n = Hill\ coefficient$$

$${K_A}^n = concentration\ of\ PLS\ at\ 50\%\ acin\ bundled$$

Binding reactions were fit to the binding isotherm equation:

$$Fraction\ PLS\ bound = \frac{P + A + K_d - \sqrt{(P + A + K_d)^2 - 4PA}}{2P}$$

$$P = concentration\ of\ PLS$$

$$A = concentration\ of\ actin$$

4.6 Differential Scanning Fluorimetry (DSF)

Recombinant plastins were diluted to 3 μM in storage buffer in the presence of Sypro Orange dye (1:5000 final dye concentration, Invitrogen). Sypro Orange is an environmentally sensitive dye with low fluorescence intensity in aqueous conditions, which highly increases in the hydrophobic environment (e.g., when bound to hydrophobic protein regions exposed upon thermal denaturation of the protein samples (4-98°C)). Changes in fluorescence of the dye were measured using a CFX Real-Time PCR Detection System (Bio-Rad) in three independent experiments. Each construct's melting temperature (T_m) was determined as the x-value of the maximum first derivative of each normalized curve, and reported as the average of the three independent trials ± standard error (SE).

4.7 Light Scattering Coupled to Ca^{2+} Titrations

The Ca^{2+} sensitivity of each PLS3 mutant was measured at a 90° incident angle by using a PTI QuantaMaster 400 spectrofluorometer (Horiba). Excitation and emission wavelengths were set at 350 nm with 3 nm slits. Polymerized F-actin (5 μM) and plastin (1 μM) were mixed and incubated (overnight at 4°C, 1 hour at 20-25°C) followed by subsequent degassing under vacuum (15 min). After 1 min of initial measurements, $CaCl_2$ (corresponding with a final free Ca^{2+} concentration as previously described (Schoenmakers et. al. 1992)) was titrated incrementally and mixed. The measurements were taken for at least 1 min between the titration points and were subsequently averaged per increment. The data was normalized and reported as the average of three independent experiments ± SE, which was plotted versus free pCa in solution. The $pCa_{50\%}$ values, a readout for Ca^{2+} sensitivity of the protein evaluated, were calculated by fitting the data to a logistic curve in Origin Software (OriginLab).

References

Lodish H., Berk A., Zipursky S.L., et al. Molecular Cell Biology. 4th edition. New York: W. H. Freeman; 2000. Section 18.1, The Actin Cytoskeleton. Available from: https://www.ncbi.nlm.nih.gov/books/NBK21493/

Perrin, B. J., & Ervasti, J. M. (2010). The actin gene family: Function follows isoform. *Cytoskeleton*, *67*(10), 630–634. https://doi.org/10.1002/cm.20475

Pollard, T. D., & Craig, S. W. (1982, February 1). Mechanism of actin polymerization. *Trends in Biochemical Sciences*. Elsevier Current Trends. https://doi.org/10.1016/0968-0004(82)90076-7

Straub, F. B., & Feuer, G. (1950). Adenosinetriphosphate the functional group of actin. *BBA - Biochimica et Biophysica Acta*, *4*(C), 455–470. https://doi.org/10.1016/0006-3002(50)90052-7

Kudryashov, D. S., & Reisler, E. (2013). ATP and ADP actin states. *Biopolymers*, *99*(4), 245–256. https://doi.org/10.1002/bip.22155

Pratt, C. W., & Cornely, K. (2014). *Essential Biochemistry*. *Essential Biochemistry* (4th editio). Hoboken, NJ: John Wiley & Sons, Ltd. https://doi.org/10.1017/CBO9781107415324.004

Pollard, T. D., & Cooper, J. A. (2009, November 27). Actin, a central player in cell shape and movement. *Science*. American Association for the Advancement of Science. https://doi.org/10.1126/science.1175862

Cooper, G. M., & Hausman, R. E. (2000). The cell: a molecular approach. Sinauer Associates. *Sunderland, MA*.

Lin, C. S., Shen, W., Chen, Z. P., Tu, Y. H., & Matsudaira, P. (1994). Identification of I-plastin, a human fimbrin isoform expressed in intestine and kidney. *Molecular and Cellular Biology*, *14*(4), 2457–2467. https://doi.org/10.1128/mcb.14.4.2457

Skau, C. T., Courson, D. S., Bestul, A. J., Winkelman, J. D., Rock, R. S., Sirotkin, V., & Kovar, D. R. (2011). Actin filament bundling by fimbrin is important for endocytosis, cytokinesis, and polarization in fission yeast. *Journal of Biological Chemistry*, *286*(30), 26964–26977. https://doi.org/10.1074/jbc.M111.239004

Bartles, J. R. (2000, February 1). Parallel actin bundles and their multiple actin-bundling proteins. *Current Opinion in Cell Biology*. Current Biology Ltd. https://doi.org/10.1016/S0955-0674(99)00059-9

Mitchison, T. J., & Cramer, L. P. (1996, February 9). Actin-based cell motility and cell locomotion. *Cell*. Cell Press. https://doi.org/10.1016/S0092-8674(00)81281-7

Arpin, M., Friederich, E., Algrain, M., Vernel, F., & Louvard, D. (1994). Functional differences between L- and T-plastin isoforms. *Journal of Cell Biology*, *127*(6 II), 1995–2008. https://doi.org/10.1083/jcb.127.6.1995

Adams, A. E., Shen, W., Lin, C. S., Leavitt, J., & Matsudaira, P. (1995). Isoform-specific complementation of the yeast sac6 null mutation by human fimbrin. *Molecular and Cellular Biology*, *15*(1), 69–75. https://doi.org/10.1128/mcb.15.1.69

Lommel, M. J., Trairatphisan, P., Gäbler, K., Laurini, C., Muller, A., Kaoma, T., … Schaffner-Reckinger, E. (2016). L-plastin Ser5 phosphorylation in breast cancer cells and *in vitro* is mediated by RSK downstream of the ERK/MAPK pathway. *The FASEB Journal*, *30*(3), 1218–1233. https://doi.org/10.1096/fj.15-276311

Kamioka, H., Sugawara, Y., Honjo, T., Yamashiro, T., & Takano-Yamamoto, T. (2004). Terminal Differentiation of Osteoblasts to Osteocytes Is Accompanied by Dramatic Changes in the Distribution of Actin-Binding Proteins. *Journal of Bone and Mineral Research*, *19*(3), 471–478. https://doi.org/10.1359/JBMR.040128

Shinomiya, H. (2012). Plastin family of actin-bundling proteins: Its functions in leukocytes, neurons, intestines, and cancer. *International Journal of Cell Biology*, *2012*. https://doi.org/10.1155/2012/213492

Addario, B., Sandblad, L., Persson, K., & Backman, L. (2016). Characterisation of Schizosaccharomyces pombe α-actinin. *PeerJ*, *2016*(3), e1858. https://doi.org/10.7717/peerj.1858

Drenckhahn, D., Engel, K., Hofer, D., Merte, C., Tilney, L., & Tilney, M. (1991). Three different actin filament assemblies occur in every hair cell: Each contains a specific actin crosslinking protein. *Journal of Cell Biology*, *112*(4), 641–651. https://doi.org/10.1083/jcb.112.4.641

Diaz-Horta, O., Bademci, G., Tokgoz-Yilmaz, S., Guo, S., Zafeer, F., Sineni, C. J., … Tekin, M. (2019). Novel variant p.E269K confirms causative role of *PLS1* mutations in autosomal dominant hearing loss. *Clinical Genetics*, *96*(6), 575–578. https://doi.org/10.1111/cge.13626

Schrauwen, I., Melegh, B. I., Chakchouk, I., Acharya, A., Nasir, A., Poston, A., … Leal, S. M. (2019). Hearing impairment locus heterogeneity and identification of PLS1 as a new autosomal dominant gene in Hungarian Roma. *European Journal of Human Genetics*, *27*(6), 869–878. https://doi.org/10.1038/s41431-019-0372-y

Shinomiya, H., Hagi, A., Fukuzumi, M., Mizobuchi, M., Hirata, H., & Utsumi, S. (1995). Complete primary structure and phosphorylation site of the 65-kDa macrophage protein phosphorylated by stimulation with bacterial lipopolysaccharide. *Journal of Immunology (Baltimore, Md. : 1950)*, *154*(7), 3471–3478. Retrieved from http://www.ncbi.nlm.nih.gov/pubmed/7897227

Hagi, A., Hirata, H., & Shinomiya, H. (2006). Analysis of a Bacterial Lipopolysaccharide-Activated Serine Kinase That Phosphorylates p65/L-Plastin in Macrophages. *Microbiology and Immunology*, *50*(4), 331–335. https://doi.org/10.1111/j.1348-0421.2006.tb03801.x

Lin, C. S., Park, T., Zong Ping Chen, & Leavitt, J. (1993). Human plastin genes. Comparative gene structure, chromosome location, and differential expression in normal and neoplastic cells. *Journal of Biological Chemistry*, *268*(4), 2781–2792. Retrieved from https://www.jbc.org/content/268/4/2781.short

Riplinger, S. M., Wabnitz, G. H., Kirchgessner, H., Jahraus, B., Lasitschka, F., Schulte, B., … Samstag, Y. (2014). Metastasis of prostate cancer and melanoma cells in a preclinical in vivo mouse model is enhanced by L-plastin expression and phosphorylation. *Molecular Cancer*, *13*(1), 10. https://doi.org/10.1186/1476-4598-13-10

Kämpe, A. J., Costantini, A., Mäkitie, R. E., Jäntti, N., Valta, H., Mäyränpää, M., … Mäkitie, O. (2017). PLS3 sequencing in childhood-onset primary osteoporosis identifies two novel disease-causing variants. *Osteoporosis International*, *28*(10), 3023–3032. https://doi.org/10.1007/s00198-017-4150-9

van Dijk, F. S., Zillikens, M. C., Micha, D., Riessland, M., Marcelis, C. L. M., de Die-Smulders, C. E., … Pals, G. (2013). *PLS3* Mutations in X-Linked Osteoporosis with Fractures. *New England Journal of Medicine*, *369*(16), 1529–1536. https://doi.org/10.1056/NEJMoa1308223

Fahiminiya, S., Majewski, J., Al-Jallad, H., Moffatt, P., Mort, J., Glorieux, F. H., … Rauch, F. (2014). Osteoporosis Caused by Mutations in *PLS3* : Clinical and Bone Tissue Characteristics. *Journal of Bone and Mineral Research*, *29*(8), 1805–1814. https://doi.org/10.1002/jbmr.2208

Nishi, E., Masuda, K., Arakawa, M., Kawame, H., Kosho, T., Kitahara, M., … Izumi, K. (2016). Exome sequencing-based identification of mutations in non-syndromic genes among individuals with apparently syndromic features. *American Journal of Medical Genetics Part A*, *170*(11), 2889–2894. https://doi.org/10.1002/ajmg.a.37826

Longoni, M., Clark, R. D., Petit, F., Giampietro, P., & Pober, B. R. (2019). MISSENSE MUTATIONS IN ACTIN-BUNDLING PROTEIN PLASTIN 3 CAUSE X-LINKED MULTIPLE CONGENITAL ANOMALIES WITH DIAPHRAGMATIC HERNIA. *American Journal of Medical Genetics Part A*, *179*(4), ajmg.a.61063. https://doi.org/10.1002/ajmg.a.61063

Oprea, G. E., Kröber, S., McWhorter, M. L., Rossoll, W., Müller, S., Krawczak, M., … Wirth, B. (2008). Plastin 3 is a protective modifier of autosomal recessive spinal muscular atrophy. *Science*, *320*(5875), 524–527. https://doi.org/10.1126/science.1155085

Schwebach, C. L., Agrawal, R., Lindert, S., Kudryashova, E., & Kudryashov, D. S. (2017). The Roles of Actin-Binding Domains 1 and 2 in the Calcium-Dependent Regulation of Actin

Filament Bundling by Human Plastins. *Journal of Molecular Biology*, *429*(16), 2490–2508. https://doi.org/10.1016/j.jmb.2017.06.021

Janji, B., Giganti, A., De Corte, V., Catillon, M., Bruyneel, E., Lentz, D., … Friederich, E. (2006). Phosphorylation on Ser5 increases the F-actin-binding activity of L-plastin and promotes its targeting to sites of actin assembly in cells. *Journal of Cell Science*, *119*(9), 1947–1960. https://doi.org/10.1242/jcs.02874

Henning, S. W., Meuer, S. C., & Samstag, Y. (1994). Serine phosphorylation of a 67-kDa protein in human T lymphocytes represents an accessory receptor-mediated signaling event. *Journal of Immunology (Baltimore, Md. : 1950)*, *152*(10), 4808–4815. Retrieved from http://www.ncbi.nlm.nih.gov/pubmed/7909824

Morley, S. C. (2012). The actin-bundling protein L-plastin: A critical regulator of immune cell function. *International Journal of Cell Biology*. https://doi.org/10.1155/2012/935173

Hornbeck, P. V., Kornhauser, J. M., Tkachev, S., Zhang, B., Skrzypek, E., Murray, B., … Sullivan, M. (2012). PhosphoSitePlus: A comprehensive resource for investigating the structure and function of experimentally determined post-translational modifications in man and mouse. *Nucleic Acids Research*, *40*(D1). https://doi.org/10.1093/nar/gkr1122

Yanyan, C., Yujin, Q., Jinli, B., Yuwei, J., Hong, W., & Fang, S. (2014). Correlation of PLS3 expression with disease severity in children with spinal muscular atrophy. *Journal of Human Genetics*, *59*(1), 24–27. https://doi.org/10.1038/jhg.2013.111

Ralser, M., Nonhoff, U., Albrecht, M., Lengauer, T., Wanker, E. E., Lehrach, H., & Krobitsch, S. (2005). Ataxin-2 and huntingtin interact with endophilin-A complexes to function in plastin-associated pathways. *Human Molecular Genetics*. https://doi.org/10.1093/hmg/ddi321

van Dijk, F. S., Cobben, J. M., Kariminejad, A., Maugeri, A., Nikkels, P. G. J., van Rijn, R. R., & Pals, G. (2011). Osteogenesis Imperfecta: A Review with Clinical Examples. *Molecular Syndromology*, *2*(1), 1–20. https://doi.org/10.1159/000332228

Forlino, A., Cabral, W. A., Barnes, A. M., & Marini, J. C. (2011, September 14). New perspectives on osteogenesis imperfecta. *Nature Reviews Endocrinology*. Nature Publishing Group. https://doi.org/10.1038/nrendo.2011.81

Donahoe, P. K., Longoni, M., & High, F. A. (2016, October 1). Polygenic Causes of Congenital Diaphragmatic Hernia Produce Common Lung Pathologies. *American Journal of Pathology*. Elsevier Inc. https://doi.org/10.1016/j.ajpath.2016.07.006

Keijzer, R., & Puri, P. (2010). Congenital diaphragmatic hernia. *Seminars in Pediatric Surgery*, *19*(3), 180–185. https://doi.org/10.1053/j.sempedsurg.2010.03.001

Ameis, D., Khoshgoo, N., & Keijzer, R. (2017). Abnormal lung development in congenital diaphragmatic hernia. *Seminars in Pediatric Surgery*, *26*(3), 123–128. https://doi.org/10.1053/j.sempedsurg.2017.04.011

Yorgan, T. A., Sari, H., Rolvien, T., Windhorst, S., Failla, A. V., Kornak, U., … Schinke, T. (2020). Mice lacking plastin-3 display a specific defect of cortical bone acquisition. *Bone*, *130*, 115062. https://doi.org/10.1016/j.bone.2019.115062

Dor-On, E., Raviv, S., Cohen, Y., Adir, O., Padmanabhan, K., & Luxenburg, C. (2017). T-plastin is essential for basement membrane assembly and epidermal morphogenesis. *Science Signaling*, *10*(481). https://doi.org/10.1126/scisignal.aal3154

Niesen, F. H., Berglund, H., & Vedadi, M. (2007). The use of differential scanning fluorimetry to detect ligand interactions that promote protein stability. *Nature Protocols*, *2*(9), 2212–2221. https://doi.org/10.1038/nprot.2007.321

Giannone, G., Rondé, P., Gaire, M., Beaudouin, J., Haiech, J., Ellenberg, J., & Takeda, K. (2004). Calcium rises locally trigger focal adhesion disassembly and enhance residency of focal adhesion kinase at focal adhesions. *Journal of Biological Chemistry*, *279*(27), 28715–28723. https://doi.org/10.1074/jbc.M404054200

Schwebach, C. L., Kudryashova, E., Zheng, W., Orchard, M., Smith, H., Runyan, L. A., Egelman, E. H., & Kudryashov, D. S. (in press). Osteogenesis imperfecta mutations in plastin 3 lead to impaired calcium regulation of actin bundling. *Bone Research*. https://doi.org/10.1038/s41413-020-0095-2

Merrell, A. J., & Kardon, G. (2013). Development of the diaphragm - a skeletal muscle essential for mammalian respiration. *FEBS Journal*, *280*(17), 4026–4035. https://doi.org/10.1111/febs.12274

Diener, A., Nebe, B., Lüthen, F., Becker, P., Beck, U., Neumann, H. G., & Rychly, J. (2005). Control of focal adhesion dynamics by material surface characteristics. *Biomaterials*, *26*(4), 383–392. https://doi.org/10.1016/j.biomaterials.2004.02.038

Tate, M. L. K., Adamson, J. R., Tami, A. E., & Bauer, T. W. (2004, January 1). The osteocyte. *International Journal of Biochemistry and Cell Biology*. Elsevier Ltd. https://doi.org/10.1016/S1357-2725(03)00241-3

Galli, C., Passeri, G., & Macaluso, G. M. (2010). Osteocytes and WNT: the Mechanical Control of Bone Formation. *Journal of Dental Research*, *89*(4), 331–343. https://doi.org/10.1177/0022034510363963

Spudich, J., & Susm WATT, A. (1971). The Regulation of Rabbit Skeletal Muscle Contraction. *J. Biol. Chem*, *246*, 4866–4871. Retrieved from https://www.jbc.org/content/246/15/4866.short

Schoenmakers, T. J. M., Visser, G. J., Flik, G., & Theuvenet, A. P. R. (1992). CHELATOR: An improved method for computing metal ion concentrations in physiological solutions. *BioTechniques*, *12*(6), 870-872, 874, 876, 878.